Phase synchronization in the forced Lorenz system

Eun-Hyoung Park, Michael A. Zaks, and Jürgen Kurths
Institute of Physics, Potsdam University, Postfach 601553, D-14415 Potsdam, Germany
(Received 3 May 1999)

We demonstrate that the dynamics of phase synchronization in a chaotic system under weak periodic forcing depends crucially on the distribution of intrinsic characteristic times of this system. Under the external periodic action, the frequency of every unstable periodic orbit is locked to the frequency of the force. In systems which in the autonomous case displays nearly isochronous chaotic rotations, the locking ratio is the same for all periodic orbits; since a typical chaotic orbit wanders between the periodic ones, its phase follows the phase of the force. For the Lorenz attractor with its unbounded times of return onto a Poincaré surface, such state of perfect phase synchronization is inaccessible. Analysis with the help of unstable periodic orbits shows that this state is replaced by another one, which we call ''imperfect phase synchronization,'' and in which we observe alternation of temporal segments, corresponding to different rational values of frequency lockings.
[S1063-651X(99)12212-8]

PACS number(s): 05.45.−a, 0.545.Xt

I. INTRODUCTION

Recent years have witnessed a strong increase of interest in different manifestations of synchronization in various physical, chemical, and biological environments. Synchronization is commonly understood as adjustment of the states of coupled systems. In the case of a strong coupling the motions in different subsystems can completely mimic each other; a weaker coupling can adjust typical time scales of the coupled systems without achieving the full coincidence between their states. In its traditional form conceived over three centuries ago [1], synchronization refers to ensembles of (two and more) periodic oscillators with slightly different individual frequencies; here, the weak coupling drives the individual frequencies together or, in general, makes them commensurable [2,3]. In the last decade, when the focus of the research has moved to chaotic phenomena, the notion of synchronization has been successfully generalized for chaotic oscillators. Here one can distinguish several stages of synchronization. Thus, the complete synchronization (or, in a modified version with unilateral coupling, ''master-slave'' synchronization) refers to the situation when two identical nonlinear systems are coupled; irrespective of the difference in initial conditions, after a certain transient, their states converge [4–7]. In a more general case, the state of the led system becomes a function of the state of the leading one (''generalized synchronization'' [8–10]).

A weaker form of synchronization which does not require that one of the coupled systems follow the evolution of the other one is restricted to the adjustment of intrinsic time scales. The natural time scale which characterizes a dynamical process is the time which a system requires for an approximate return to its initial state. In terms of the motion in phase space this characteristic is given by the interval τ_{ret} between the two consecutive returns of the chaotic trajectory onto an appropriate secant surface (Poincaré surface). In general, these intervals vary over the attractor: τ_{ret} is a function of coordinates on the Poincaré plane; however in many cases the variation is small compared to the value of τ_{ret} itself, and the chaotic motion can be viewed as a nearly regular rotation with chaotically modulated amplitude. This usually holds for the attractors originating from the sequence of period-doubling bifurcations, such as one of the prototypic low-dimensional chaotic systems: the Rössler attractor. A relatively weak periodic force applied to such a system can impose its rhythm on the rotations without destroying the erratic nature of the motion: although the returns onto the Poincaré surface are adjusted to the period of the force, the mapping of this surface onto itself, induced by the flow, remains chaotic. Since the temporal characteristics of rotations are their phase and frequency, this form of synchronization is called ''phase synchronization'' [11].

There are several ways to extend the notion of the phase in order to enable its usage in the context of chaotic processes. Since the phase usually is not available as a direct observable, some operational definition is necessary, which would allow one to reconstruct it from the experimental or numerical data. It is natural to require that the properly introduced phase as a function of time should grow ''on the average,'' and its net increment between each two consecutive intersections of the orbit with the Poincaré plane should be close to a constant (it is often convenient to scale this constant to 2π or 1). One of the commonly accepted methods to visualize the phase is to consider the ''analytic signal'' introduced by Gabor [12], and to decompose a time series into the instantaneous phase and instantaneous amplitude by means of the Hilbert transform. In certain situations, due to the geometry of the attractor, rotations are clearly visible on phase portrait projections; this prompts a simpler choice: given the ''rotation center,'' we view the phase as a time-dependent angular polar coordinate on the phase plane. Perhaps, the most straightforward and crude approach would be to define the phase by prescribing its values at the moments of the intersection of the orbit with the Poincaré surface. Let us assign the value 2π to the phase increment after each turn. If now we admit the linear interpolation between the intersection moments, the phase is rendered as a monotonic piecewise-linear function of time: let t_k be the moment of the kth intersection of the orbit with the surface of section;

then for $t_k \leqslant t \leqslant t_{k+1}$ the phase is simply $\Phi(t) = 2\pi k + 2\pi(t-t_k)/(t_{k+1}-t_k)$.

For practical purposes of synchronization, all these definitions of phase appear to be equally applicable [13]. Given the phase, the mean frequency of the chaotic motion is introduced as the mean growth rate of the phase, averaged over the attractor.

Below, we focus on the onset of synchronization in periodically driven chaotic systems; this situation may be viewed as a particular case of unilateral coupling in which the driving subsystem performs periodic oscillations whereas the driven one exhibits chaotic behavior. Under the action of the periodic force, the typical time scales of the chaotic attractor can get adjusted to the imposed period of oscillations. It is natural to expect that in the synchronized state the phase of the chaotic motion would follow that of the driving force; correspondingly, the forcing frequency should coincide with the mean frequency of the chaotic observable. This phenomenon has been documented for driven systems whose characteristic times are confined within a relatively narrow range (see, e.g., [14,15]).

However, one often encounters continuous dynamical systems in which the band of characteristic times is rather broad or even (semi-)infinite; the latter happens, e.g., when the closure of a chaotic attractor contains fixed points of the saddle type. In this case τ_{ret} diverges near the local stable manifold of the saddle point. Situations in which the unstable steady states (imaged in the phase space by saddle points) play an important role in dynamics are widely spread in finite-dimensional truncations of the equations of nonlinear optics (Raman scattering [16], lasers with saturable absorbers [17], optothermal devices [18]), thermal convection in certain configurations [19–21], or reductions of the weakly dissipative one- and two-dimensional complex Ginzburg-Landau equation near the boundary of the modulational instability [22,23]. The best known example is provided by the Lorenz attractor [24]: here, in the course of chaotic evolution the relatively fast rotations around the unstable focal points in phase space alternate with slowing down and long hoverings near the saddle point.

In this paper, we consider the externally driven Lorenz system in order to investigate the influence of unbounded return times on details of phase synchronization. For comparison, we take two sets of parameters, the first one describing the ''canonical'' Lorenz attractor containing the saddle point [24] and the second one corresponding to a qualitatively different kind of an attractor with narrow distribution of τ_{ret}.

We intend to describe the synchronization phenomena in terms of unstable periodic orbits embedded into a strange attractor. These orbits constitute a kind of a ''skeleton'' for chaotic sets [25], and knowledge of their properties allows us to resolve many fine details of an attractor in terms of the cycle expansion [26–29], to compute its fractal dimensions [30], etc. Unstable periodic orbits have been widely exploited in the context of chaotic sets in mappings and flows; they provide a helpful tool for analyzing experimental data [31–35]; recently the algorithms were elaborated to recover them in numerical solutions of the partial differential equations [36]. Finally, knowledge of these orbits allows us to proceed from the passive observation of chaotic process to the active interference into dynamics: one can control chaos [37] by adding small local perturbations which stabilize the otherwise unstable periodic motions.

The Lorenz attractor which possesses an infinite number of periodic solutions with two-dimensional unstable manifolds has been several times analyzed by means of unstable periodic orbits [38,39]. Characterization of the Lorenz system in terms of these orbits has certain peculiarities. For many dynamical systems, tracking only several relatively short unstable periodic orbits seems to be sufficient in order to obtain a good approximation to the properties of the attractor [40]. However, in systems close to the attractor crises (of which the Lorenz attractor is a good example) some effects become visible only when one investigates orbits with progressively increasing length [41,42].

We find that the presence of the broadband of characteristic times brings new features into synchronization-related phenomena. According to our results, in such systems it seems impossible to achieve the state of perfect phase synchronization for which the frequency of the driving force would identically coincide with the mean frequency on the attractor. We observe that during the chaotic evolution long segments of perfectly synchronized motion alternate with short segments during which the external force lags behind the chaotic rotations. A closer look shows that the latter events correspond to the passage of the trajectory near certain long periodic orbits. A detailed investigation demonstrates that even at this stage the system remains phase synchronized; however, this is a ''masked'' synchronization caused by higher resonances: the frequencies do not coincide but are commensurate.

The layout of our paper is as follows. In the next section we describe the system under investigation and introduce the main characteristics to be computed. Further, we provide a brief general survey of phase synchronization in terms of unstable periodic orbits. Section III presents the bifurcation diagram for the case when the return times on the attractor are confined within a narrow interval (the parameter r of the Lorenz equations equals 210). The results displayed in Sec. IV refer to the forced system at $r=28$; here we describe the changes which are introduced into the picture of phase synchronization by unbounded return times.

II. DRIVEN LORENZ EQUATIONS: PHASE AND PERIODIC ORBITS

We consider the Lorenz system [24] driven by an external force. The dynamics of dimensionless variables x,y,z is governed by the equations

$$\begin{aligned} \dot{x} &= \sigma(y-x), \\ \dot{y} &= rx - y - xz, \\ \dot{z} &= xy - bz + E\cos(\Omega t), \end{aligned} \tag{1}$$

where σ, r, and b are the original Lorenz parameters, and the dimensionless amplitude and frequency of the external force are denoted by E and Ω, respectively. To preserve the characteristic mirror symmetry of the equations, the forcing term is applied to the third variable. We fix the ''canonical'' [24]

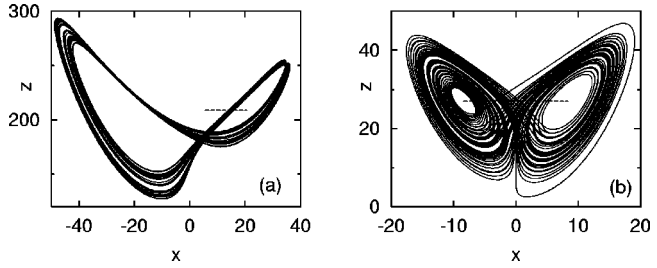

FIG. 1. Chaotic orbits of Eq. (1) for (a) $r=210$ and (b) $r=28$. Dashed line: location of the Poincaré surface $z=r-1$.

parameter values $\sigma=10$ and $b=8/3$. As for the parameter r, we take two values which correspond in the autonomous system to two qualitatively different types of a chaotic attractor [Figs. 1(a) and 1(b)]: the nearly isochronous one and the strongly nonisochronous one. We expect that the difference in the distribution of intrinsic time scales should influence the way in which the system reacts to the synchronizing action of the external force.

In the first case $r=210$, we do not foresee particular differences from the earlier studied example of the forced Rössler system [14]; it serves as a convenient illustration of metamorphoses in phase space which accompany the phase synchronization. The second case, the classical Lorenz attractor at $r=28$, is more complicated, since here the time between two consecutive intersections of the secant plane by a trajectory is, in principle, unbounded. In both cases the values of amplitude which we take ($E\leqslant 20$ for $r=28$ and $E\leqslant 10$ for $r=210$) are small compared to the maximal values of dz/dt in the autonomous system (~ 350 and ~ 3500, respectively), and the introduced perturbations can be viewed as relatively weak.

Since we focus on phase synchronization, the phase of the motion should be defined properly. There are several ways to introduce the phase (see, e.g., the three definitions in [11]). Insofar as we are interested in long-time effects, the details within a single turn of the trajectory do not seem to be of special importance. For this reason, we choose the simplest and the most robust characteristics: as proposed in the Introduction, we infer the phase from the geometry of the orbit. It is natural to assume that each new turn of the orbit should add 2π to the phase ϕ. By the ''turn'' we denote the segment of the orbit between two consecutive intersections of the suitably chosen secant surface. The latter can be selected in several ways. In order to escape the ambiguity which may arise from the clockwise and counterclockwise rotations on the two opposite lobes of the Lorenz attractor, one can choose, e.g., the surface on which dz/dt in the unperturbed system vanishes. Following the original work of Lorenz [24], we take a different choice: we define the Poincaré surface by the condition $z=r-1$ and count the intersections at which dz/dt is negative.

Respectively, the mean frequency (which is the mean time derivative of the phase) at the attractor can be computed through any of the two apparently equivalent expressions: either as

$$\omega=\lim_{T\to\infty}\frac{2\pi N(T)}{T}, \tag{2}$$

where $N(T)$ is the number of turns performed in the time T, or, conversely, as

$$\omega=\lim_{N\to\infty}\frac{2\pi N}{T(N)}, \tag{3}$$

where $T(N)$ is the time required to complete N turns. Naturally, the details of the phase evolution within a single turn cannot be captured by such a crude construction; the price which we pay is an inaccuracy in ϕ bounded by $\pm 2\pi$ and, respectively, an error in the estimate of ω bounded by the value $\pm\omega/N$.

Along with the averaged characteristics, we should also introduce quantities which characterize every particular periodic orbit embedded into the attractor. For the periodic orbit which closes after the time T_0 and consists of N_0 turns (following [14], we call this integer number the ''orbit length'' or simply ''length'') its individual frequency is provided by any of the expressions (2) and (3) without the necessity to take the limit:

$$\omega_i=\frac{2\pi N_0}{T_0}. \tag{4}$$

An indispensable tool for studies of chaotic sets, unstable periodic states have for our purpose yet another merit: each of them can be viewed as an individual oscillator. Let us pick up one of these solutions and consider, first, the dynamics on its global stable manifold. This brings us back to the well-studied problem of the synchronization of *stable* periodic oscillations by external force. The introduction of periodic forcing increases the dimension and changes the topology of the phase space. Provided the forcing is weak enough (which we will assume throughout our analysis), an invariant smooth torus evolves from the closed curve of the autonomous chaotic system, and the orbits wind on this torus.

In parameter space, phase entrainment is observed in certain ''locking'' regions (the Arnold tongues) which correspond to rational values of the ratio between the driving frequency Ω and the individual frequency ω_i of the considered periodic orbit. Usually, only the main tongue in which the frequencies coincide is of relevance for applications. Inside each Arnold tongue, there are two closed orbits on the surface of the invariant torus: the attracting one (it is natural to call it ''phase stable'') and the repelling one (respectively, ''phase unstable''); on the edge of the tongue these two orbits coalesce and disappear via the tangent bifurcation. Outside the tongues the motion is not synchronized, and the trajectories are dense on the torus.

Now let us leave the stable manifold of the individual periodic orbit and consider dynamics in the entire phase space. On the parameter plane of the frequency Ω and amplitude E of the driving force, the main Arnold tongue emanates from the point $E=0$, $\Omega=\omega_i$. Naturally, the individual frequencies ω_i differ for different periodic orbits of the autonomous systems; if they are close to each other, the main Arnold tongues of these orbits overlap; moreover, a parameter region common to all these tongues can exist, in which the phases of all periodic motions are locked to the phase of external force. If the forcing remains moderate, this is the overlapping region for the leftmost and the rightmost Arnold

tongues (they correspond to the periodic motions of the autonomous system with, respectively, the lowest and the highest values of ω_i). Since in the autonomous system each periodic solution is unstable, the corresponding torus in the weakly driven system is also unstable. Chaotic trajectories in their motion over the attractor repeatedly visit the neighborhoods of the tori. Near a torus, the orbit approaches the respective phase-stable solution and moves along it before the ''transverse'' (amplitude) instability repels it to another torus. Inside the overlapping region, the phase-stable solution on each torus is phase locked with the external force in the ratio 1:1; therefore the perfect phase synchronization is observed. Owing to the noncoincidence of Arnold tongues for different periodic orbits, just outside the region of phase synchronization the synchronized segments of the trajectory alternate with the nonsynchronized ones. This specific kind of intermittency has been called ''eyelet,'' because each escape from the phase-locked state is caused by the very precise hitting of a neighborhood of a nonlocked torus [43].

Since the characteristic multipliers (eigenvalues of the linearization of the Poincaré map near the fixed point) of periodic orbits are readily available in computations, it can prove helpful to relate them to the phenomena which we expect to observe in the course of our study. In the absence of an external force each periodic orbit has two multipliers. None of these orbits is stable; this means that at least one of the multipliers should lie outside the unit circle on the complex plane. Simple arguments show that this multiplier is real; in the case $r=28$ it is positive, and in the case $r=210$ it can be either positive or negative. The second multiplier (which corresponds to the decaying perturbations) is also real and lies close to zero. When the system is driven by the external force, the dimension of the phase space is increased and an additional multiplier appears; under small amplitudes of forcing it characterizes the adjustment of the own phase of the system to the phase of the external force. If the forcing is weak, the phase evolution is decoupled from the amplitude dynamics, and all three multipliers remain real. Formally one may extend the description to the autonomous case $E=0$; in this case the system is nonsensitive to the external phase, the direction in the phase space corresponding to its change is marginal (the torus is foliated into a continuum of closed curves), and the multiplier equals 1. As soon as a nonzero forcing is introduced, this degeneracy is destroyed; of all the closed curves survive either two (inside phase-locked regions) or one (on their boundaries) or none (outside the Arnold tongues). Inside a phase-locking region, the third multiplier for the phase-stable orbit lies between 0 and 1, and for the phase-unstable orbit it is larger than 1.

We expect that in the synchronized state phase-stable orbits build a skeleton of the chaotic attractor whereas the phase-unstable ones form a backbone of the repeller which separates in phase space the basins of equivalent attractors shifted with respect to each other by 2π [43,14,15]. On the edge of the phase-locking region, two orbits coalesce and disappear; an eyelet gap appears in the barrier formed by the repeller, and enables the phase drift with respect to the phase of external force. Naturally, not all the periodic orbits are obliged to belong to an attractor or repeller; some of them may lie in the region of phase space which is not visited by trajectories from the attractor; respectively, the disappearance of a pair of such orbits goes unnoticed from the point of view of the phase synchronization.

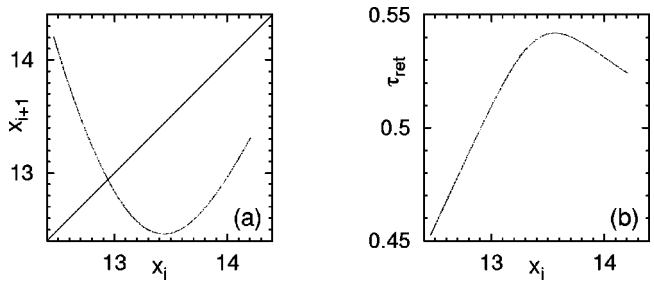

FIG. 2. (a) Return mapping and (b) return time on the Poincaré surface $z=r-1$ for $r=210$ (two turns of the orbit in the phase space).

Finally, several words about the numerics employed: to locate the periodic orbits, we use the Newton method in several variables. The periodic orbit is represented by a fixed point of the Poincaré map; this map is two dimensional in the autonomous case and three-dimensional for the driven system. To calculate on the parameter plane the boundaries of the phase-locked regions (which correspond to the tangent bifurcation of periodic orbits), we fix the driving amplitude and treat the frequency of the external force as the fourth unknown variable.

III. $r=210$: SYNCHRONIZING ALMOST ISOCHRONOUS ATTRACTOR

At $r=210$ (as well as for the other values of r between 197.4 and 215.4 [44]) the autonomous Lorenz equations have two mutually symmetric chaotic attractors. Their attraction basins in phase space are separated by the stable manifold of the saddle point which is located at the origin. The origin does not belong to either of the attractors; hence the times between consecutive returns onto the Poincaré plane are bounded. We show one of these attractors in Fig. 1(a).

Due to strong transversal contraction, the trace of the attractor on the Poincaré surface is nearly nondistinguishable from the one-dimensional curve; consequently the two-dimensional mapping induced by the flow can be for practical purposes replaced by the one-dimensional one. Furthermore, on this attractor the turns (in the above sense of orbit segments between consecutive intersections with the Poincaré plane) in the half-space $x>0$ alternate with the turns in the half-space $x<0$; after every two turns the orbit returns to the initial half-space. Therefore it is sufficient to consider the one-dimensional mapping in one of the half-spaces (naturally, keeping in mind that each iteration of this map corresponds to two turns of the orbit). Such a mapping reconstructed numerically from the x coordinate of the intersection points is presented in Fig. 2(a). This proves to be a unimodal map reminiscent of the logistic mapping $x\rightarrow ax(1-x)$; comparison of symbolic itineraries for the extrema of the two mappings shows that the dynamics observed in our system corresponds to $a\approx 3.80552\ldots$. The second part of the plot presents the return time τ_{ret} as a function of x [Fig. 2(b)]. It can be seen that variations of τ_{ret} are quite moderate.

Since we are going to interpret synchronization in terms of unstable periodic orbits, the distribution of the frequencies

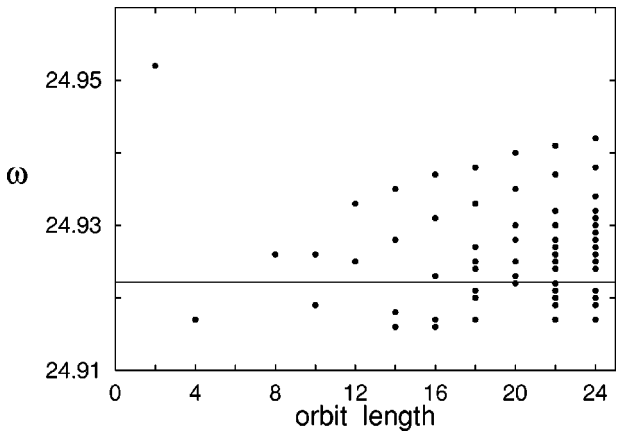

FIG. 3. Individual frequencies of periodic orbits at $r=210$. The mean frequency ω_a of autonomous chaotic motion is shown by solid line.

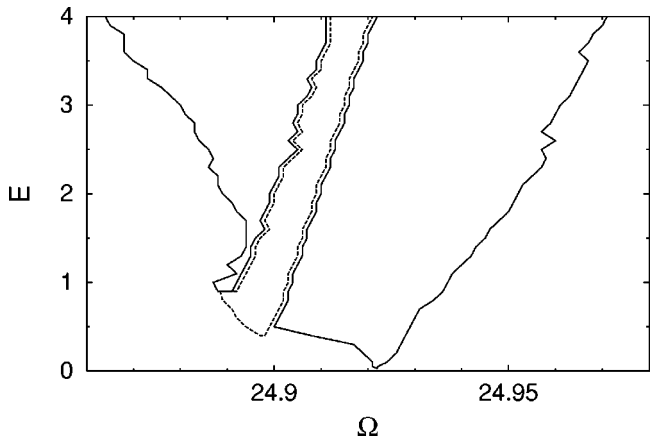

FIG. 5. Domain of phase synchronization for $r=210$. The dashed curve encircles the region of periodic dynamics.

of these orbits (4) is of obvious importance. Not all of the unstable periodic orbits existing in Eq. (1) at $r=210$, $E=0$ are embedded into the chaotic attractor; many of them (born mostly from the homoclinic explosion at $r=13.926$ [44]) are located in the other parts of the phase space and their individual frequencies are irrelevant in our context. As for the orbits belonging to the attractor, we have computed their frequencies until the orbit length 24. As can be seen from the data plotted in Fig. 3, the distribution is nearly monochromatic: the difference between the highest and the lowest frequency is less than 0.2% of the mean frequency of the autonomous chaotic motion $\omega_a=24.9222\ldots$ (the latter value is estimated from 10^7 turns of a chaotic orbit). Therefore, one can hope to synchronize the entire chaotic motion by applying a relatively weak periodic force with the frequency close to ω_a.

To detect phase synchronization in the driven system, we have computed the difference between the mean frequency of the observed chaotic motion ω and the frequency of the driving force Ω: for the synchronized state this difference should vanish. The plot in Fig. 4 presents ω-Ω as a function of Ω under a fixed value of the amplitude E; the horizontal plateau corresponds to the interval of the Ω values which

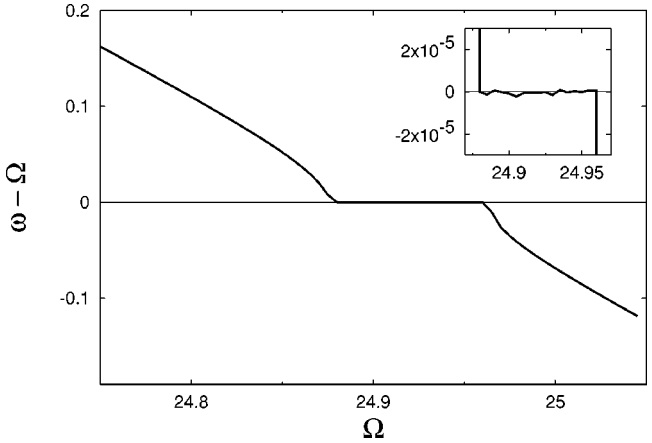

FIG. 4. Difference between mean frequency ω and driving frequency Ω for $r=210$, $E=3$. ω is estimated from 10^6 turns of chaotic orbit.

ensure the synchronization. To check for the occasional phase slips, we magnify the part of this plot around the plateau; as seen in the inset, the differences between the computed values and zero lie within the error estimate $\pm\omega/N$ for ω.

The coincidence of frequencies is a necessary condition for phase synchronization; it is not a sufficient one, since it does not exclude the weak phase drift which is slower than linear in time. Numerical observations inside the plateau did not disclose any phase drift within 10^6 turns of the orbit. This allows us to conjecture that the observed state is completely phase synchronized. Varying the value of the forcing amplitude, we determine on the plane of the parameters Ω and E the domain of phase synchronization (Fig. 5).

By itself, the condition of vanishing ω-Ω through which we determine the state of phase synchronization provides no information on the kind of synchronized behavior: it can be both chaotic and periodic. A closer look at the regimes observed inside this domain indicates that in certain parameter regions chaos yields to periodicity: there is a large window with a stable periodic orbit which makes six turns in the phase space; just outside this window stable orbits of 6×2^n turns can be encountered, and there is also a small region with stable motions of length 14. The origin of these periodic windows can be interpreted with the help of the return mapping. We mentioned already that the one-dimensional mapping induced by the flow in the autonomous system (recall that in obtaining this map only half of the orbit turns counts) appears to be equivalent to the logistic mapping at $a=3.80552\ldots$. This value is remarkably close to the $a=1+\sqrt{8}=3.8284\ldots$ which marks the lower boundary of the period-3 window in the logistic mapping; the interval $3.774\,14<a<3.774\,45$ corresponding to the period-7 window of the logistic mapping is also rather close. Apparently, weak perturbations introduced by the forcing deform the mapping and can bring it across the boundary of periodic behavior. We assume that a multitude of other periodic windows with longer periods exist inside the synchronization region; however, these windows should be rather narrow; we can hope that as long as the mapping for the variable x is well approximated by the unimodal map, the measure of the parameter values corresponding to chaotic motions remains positive.

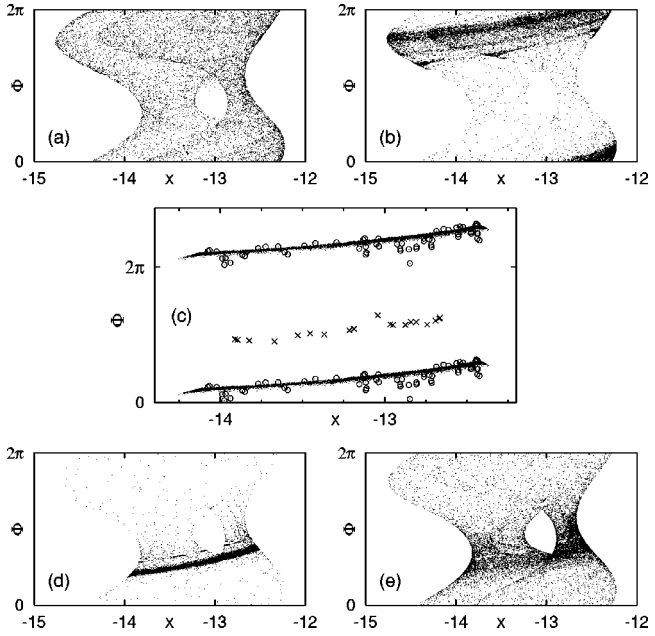

FIG. 6. Dynamics on the Poincaré surface for $r=210$, $E=3$: (a) $\Omega=24.8$, (b) $\Omega=24.877$, (c) $\Omega=24.94$, (d) $\Omega=24.963$, and (e) $\Omega=24.97$. Circles and crosses in (c) denote, respectively, phase-stable and phase-unstable orbits.

Except for these windows, the remaining part of the parameter plane is occupied by the chaotic states, phase synchronized and nonsynchronized.

The phase dynamics is illustrated by the Poincaré mapping; along with the coordinates x and y inherited from the autonomous case, an appropriate variable for this mapping is the phase ϕ of the external force at the moments of the intersection of the orbit with the secant plane $z=r-1$. In a nonsynchronized state the values of the phase are scattered over the whole range between 0 and 2π. In the synchronized regime, on the contrary, they are localized in a relatively small interval, and the attractor for the mapping appears to be a narrow stripe. Attractor projections presented in Fig. 6 correspond to the monotonic increase of the frequency Ω under the fixed amplitude; they demonstrate the transition from the nonsynchronized state [Fig. 6(a)] to the synchronized attractor [Fig. 6(c)] and subsequent breakup of synchronization [Fig. 6(e)]. In the intermediate stages [Fig. 6(b) and Fig. 6(d)] just outside the region of phase synchronization we observe the weak diffusion of the phase: its values stay in the localized domain for most of the time, but after several thousands of iterations they leave it and drift upwards (or downwards) to the identical stripe located 2π higher (respectively, lower).

Let us interpret the dynamics of phase in terms of periodic orbits. In Fig. 6(c), the attractor is presented together with unstable periodic orbits up to the length of 14; for convenience, we also show the identical attractor whose phase is shifted by 2π. As can be seen, the attractors are hemmed in by periodic orbits (shown by the circles); these are the phase-stable orbits. The phase-unstable orbits (shown by the crosses) are located halfway between the attractors; apparently, they lie on the border which separates the attraction domains.

The individual locking regions for several relatively short

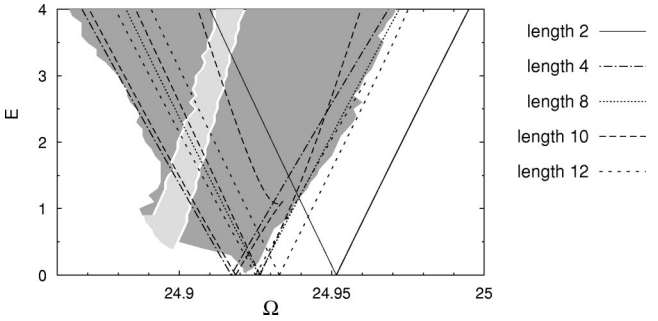

FIG. 7. Phase-locked regions for individual periodic orbits at $r=210$. Dark gray area: domain of phase-synchronized chaotic dynamics. Light gray area: stable periodic states.

periodic orbits are shown in Fig. 7. We see that (except for the windows of stable periodic behavior) the borders of the phase synchronization domain well correlate with the borders of the Arnold tongues, and phase synchronization is observed for the parameter values under which most of the periodic solutions are phase locked. Only the shortest periodic motions, those of the length 2, seem to play no role in the whole process; this can be ascribed to the fact [cf. Fig. 6(c)] that the phase-stable (phase-unstable) orbits of this period appear to be lying outside the attractor (repeller). A similar phenomenon when certain periodic orbits under the action of the external force leave the bulk of the chaotic attractor has been previously reported for the forced Rössler equations [14]. Note also the cusp point on the right border of the Arnold tongue for one of the orbits of length 10: it owes to the transcritical bifurcation in which two orbits of this length from different Arnold tongues participate; this event, noteworthy by itself, seems to have no effect on phase synchronization.

IV. $r=28$: IMPERFECT PHASE SYNCHRONIZATION OF THE LORENZ ATTRACTOR

The picture of phase synchronization at $r=28$ differs noticeably from the one reported in the preceding section. The reasons for this can be traced back to the autonomous case $E=0$. In the absence of force, we have the familiar Lorenz attractor [24] [Fig. 1(b)]. It is well established that the saddle point located at the origin $x=y=z=0$ belongs to the closure of the attractor. The influence of this fact on the dynamics can be conveniently illustrated by means of return map and return times. Strong contraction effectively reduces the two-dimensional mapping on the Poincaré plane $z=r-1$ to a nearly one-dimensional (1D) one (the transverse Cantor structure of the 2D map appears to be of no importance for our purposes) which maps two curves onto themselves. Introducing the appropriate coordinate along these curves (see, e.g., [44]) one arrives at the discontinuous mapping of the line onto itself; the discontinuity corresponds to the intersection of the Poincaré plane by the local stable manifold of the saddle point. The orbits which belong to the local stable manifold never return back to the secant surface, and the orbits which cross the Poincaré plane near the trace of this manifold hover for a long time in the vicinity of the origin. Owing to this, the time required for one turn on the attractor is not bounded from above; as a function of the mapping

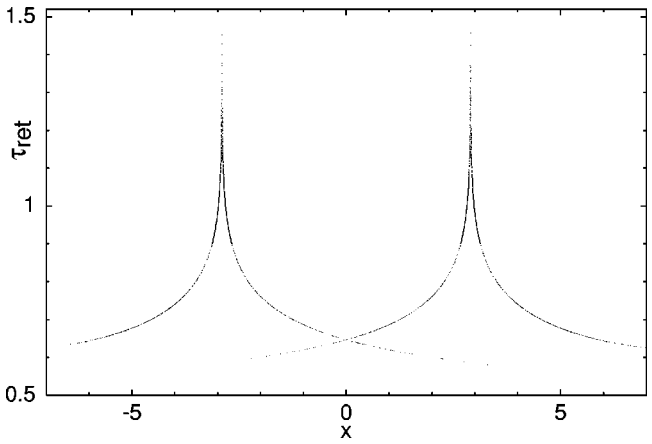

FIG. 8. Return time at the Poincaré surface $z=r-1$, $r=28$. Two branches correspond to the two lobes of attractor.

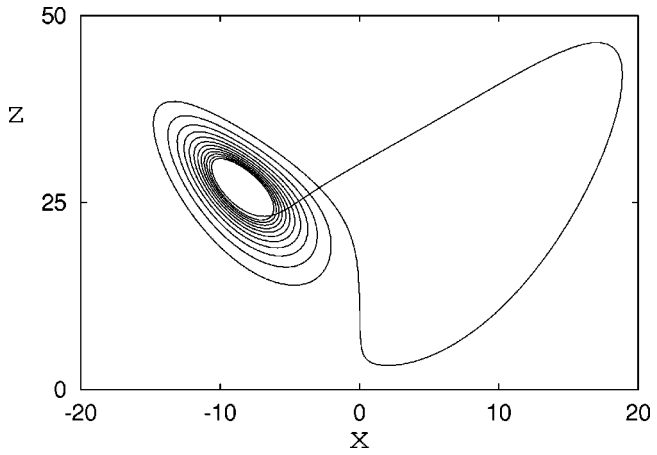

FIG. 10. Unstable periodic orbit of length 13 with the largest individual frequency.

coordinate, it diverges logarithmically when approaching the discontinuity (Fig. 8).

To a certain extent this is compensated by the geometry of attractor: after hovering near the origin, the trajectories are reinjected close to the unstable saddle-focus points $[x=y=\pm\sqrt{b(r-1)}, z=r-1]$ where the rotation is especially fast, so that typically a slow turn is followed by a sequence of relatively rapid ones.

To get an idea of the distribution of characteristic times in the nonforced system, we located all its unstable periodic orbits up to the length of 19. The distribution of individual frequencies for these orbits is shown in Fig. 9.

We observe that (unlike the case of $r=210$; cf. Fig. 3) the span between the highest and the lowest values of individual frequencies chosen among all the orbits of the length l grows with the increase of l. The growth of the maximal value of ω_i is limited from above. The highest frequency of rotations in the phase space appears to be attained near the saddle focus points; it is bounded by the imaginary part of the complex eigenvalues of the Jacobi matrix at these points which, for the parameter employed, equals 10.1945 . . . . However this value remains unreachable for periodic trajectories: since the saddle foci lie outside the attractor, periodic and chaotic orbits pass at a finite distance from them. In the course of time

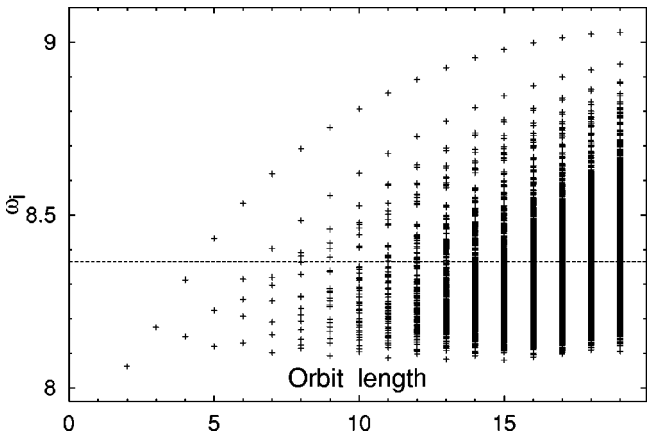

FIG. 9. Individual frequencies of periodic orbits at $r=28$. The mean frequency ω_a of autonomous chaotic motion is shown by the solid line.

evolution, an orbit can make only a finite number of subsequent rotations around one of the saddle foci before slowing down and leaving for the other half-space (according to [44], this number for $r=28$ does not exceed 33).

A bit surprisingly, due to the mentioned compensation effect, the upper branch in Fig. 9 corresponds precisely to the orbits which come on the nearest to the origin and, hence, experience the strongest slowdown: as seen in Fig. 10, such an orbit of length l makes a single turn in the half-space $x>0$ (or $x<0$) and $l-1$ turns in the half-space $x<0$ (respectively, $x<0$).

Regarding the minimal value of ω_i for the periodic orbits, the following argument shows that it can lie arbitrarily close to zero. It is known that the values of r which correspond to the formation of secondary (multiturned) homoclinic orbits are dense in the range $24.06<r\leqslant 33$ [44]. Consequently, arbitrarily close to $r=28$ one can find homoclinic explosions from which the new unstable periodic orbits are created; due to proximity to the corresponding bifurcation points, the periods of these orbits at $r=28$ can be arbitrarily large and, hence, their frequencies arbitrarily low. However, the very same proximity to bifurcation points makes these orbits extremely unstable and, thereby, hardly relevant for the dynamics on the attractor. Near the bifurcational value r_0 corresponding to the homoclinic explosion, the characteristic multiplier responsible for the instability is proportional to $(r-r_0)^\nu$ where $\nu=(\lambda_u+\lambda_s)/\lambda_s$ is a combination of the unstable eigenvalue λ_u and the least stable eigenvalue λ_s of the fixed point at the origin [45]. Linearization of the equations under the employed parameter values yields $\nu=(49-3\sqrt{1201})/16\approx -3.44$. Correspondingly, the positive Lyapunov exponent of this periodic orbit (which is simply the logarithm of its characteristic multiplier) scales as $\nu\ln(r-r_0)$ and diverges at r_0. Since the weight of the contribution of an unstable periodic orbit to chaotic dynamics is inversely proportional to the Lyapunov exponent of this orbit [30,39], it is obvious that close to the homoclinic explosion such a contribution is negligible. Besides, our calculations show that in the interval $27<r<29$ the first 26 symbols in the symbolic itinerary of the unstable manifold of the origin [44] do not change; accordingly, homoclinic bifurcations with the number of turns smaller than 25 do not occur inside this interval; consequently, the periodic orbits with anomalously

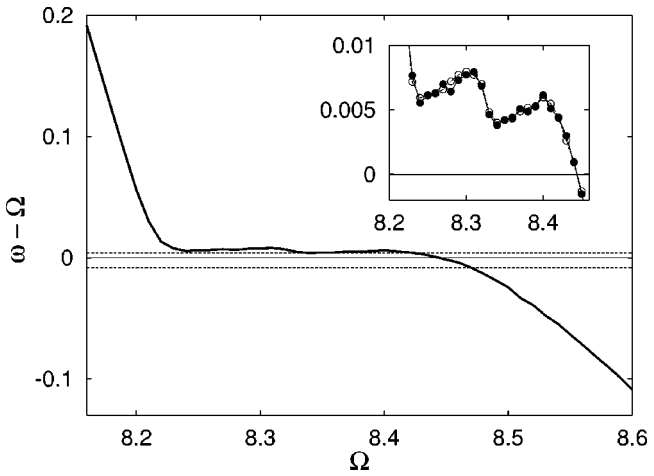

FIG. 11. Difference between mean frequency ω and driving frequency Ω estimated from 10^6 (solid circles) and 10^7 (open circles) turns of chaotic orbit; $r=28$, $E=10$.

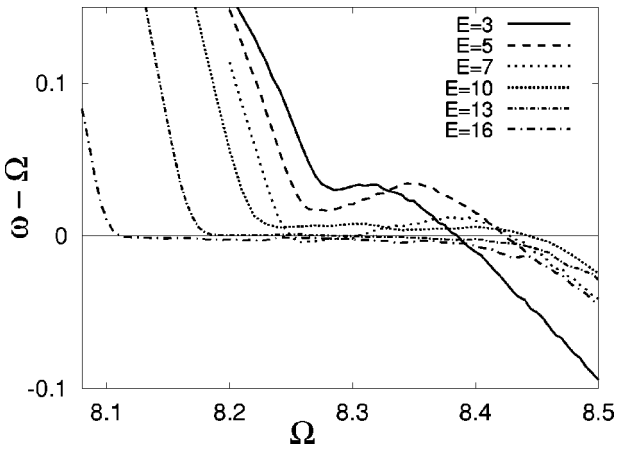

FIG. 12. Plateaus of imperfect phase synchronization for different amplitudes of external force.

low frequencies which can be met there, should have large lengths.

We can conclude that the band of individual frequencies for the periodic orbits with short and moderate lengths is bounded both from below and from above. Nevertheless, variation in the frequencies is remarkably large: the difference between the highest and the lowest marks exceeds 11% of the mean frequency $\omega_a=8.365\ldots$ [the latter value is obtained by applying the expression (3) to the chaotic trajectory averaged over the length of $N=10^7$ turns]. Taking into account the broad scattering of the typical times of the system, it is intuitively clear that synchronizing all of them by a weak external forcing is not an easy task.

To check for phase synchronization, we use the same criterion as in the preceding section: the difference between the mean frequency ω on the attractor and the frequency Ω of the driving force. Fixing the forcing amplitude E we scan the range of the values of Ω searching for vanishing or nearly vanishing values of $\omega-\Omega$. Typical results are presented in Fig. 11; here, $E=10$. From the first view, the horizontal plateau seems to indicate to the perfect phase synchronization. However, a closer look (cf. the inset in Fig. 11) shows that the plateau is, first, not exactly horizontal, and, second, lies at a small but finite distance above zero. The latter circumstance cannot be attributed to insufficient statistics caused by the low number of orbit turns N: the estimates from $N=10^6$ and $N=10^7$ as plotted in the inlet, match pretty well.

Similar results are obtained for other values of the driving amplitude (Fig. 12). For each fixed value of $E>2$ there appears to be an interval of values of the driving frequency around ω_a in which $\omega-\Omega$ as a function of Ω is nondecreasing or decreases very weakly.

These (not always horizontal) plateaus can be located above zero ($E<14$) or below zero ($E\geqslant 14$), but invariably close to it: in each of them the value of $\varepsilon\equiv|\omega-\Omega|/\Omega$ is everywhere smaller than 0.01. Numerical observations indicate that here the trajectory can be separated into alternating synchronized and nonsynchronized segments, so that its phase follows the phase of the driving phase in the former and departs from it in the latter. In the rough assumption that each new 2π increment of the phase difference is gained within a single nonsynchronized turn of the orbit, the value of ε provides a ratio between the number of nonsynchronized turns, N_n, and that of the synchronized turns, N_s: $|\varepsilon|\cong N_n/N_s$. The smallness of ε inside the plateaus confirms that the synchronized segments prevail within a single chaotic orbit. This permits us to view the corresponding states as ''nearly'' synchronized; delineating the region of plateaus on the parameter plane, we obtain the domain of imperfect phase synchronization. Naturally, owing to a certain arbitrariness in determination of the plateau end points, the borders of this domain are somewhat fuzzy.

Again, the dynamics of phase is captured by the Poincaré mapping. Unlike the case of the previous section, the mapping attractor never resembles a stripe which is localized in the phase variable ϕ. Let us fix a value of the forcing amplitude and traverse the region of imperfect synchronization by increasing the value of the driving frequency. Along this line in the parameter space, the attractor exhibits the transformation from a diffuse cloud [Fig. 13(a)] into reasonably well outlined patterns of Figs. 13(b) and 13(c) and further into a diffuse set depicted in Fig. 13(d). In the most ordered pattern [Fig. 13(c)] one can distinguish the heavily populated central region (which spreads over approximately half of the

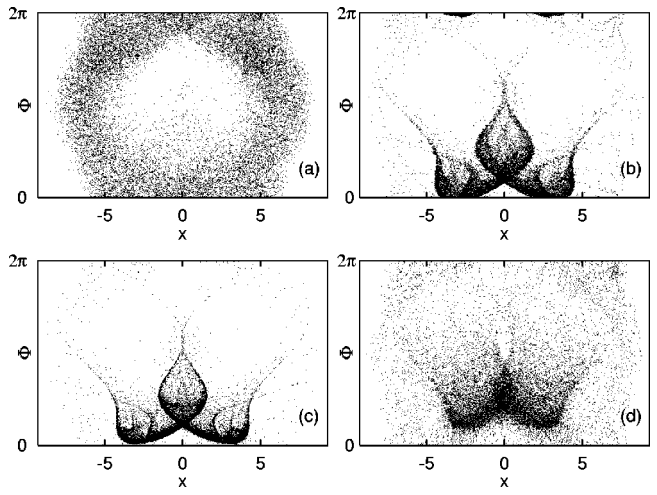

FIG. 13. Attractors of the Poincaré mapping at $r=28$, $E=10$: (a) $\Omega=7.5$, (b) $\Omega=8.3$, (c) $\Omega=8.35$, and (d) $\Omega=8.5$.

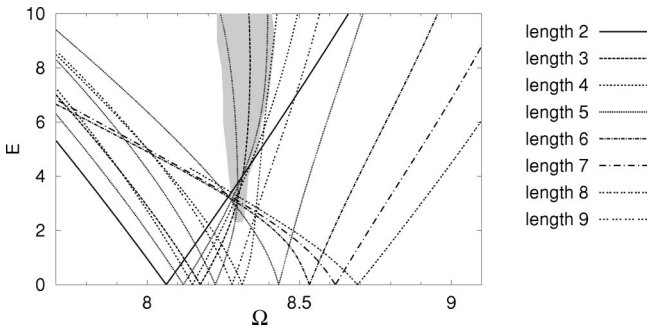

FIG. 14. Main phase-locked regions of individual periodic orbits; $r=28$. Gray domain: region of imperfect phase synchronization.

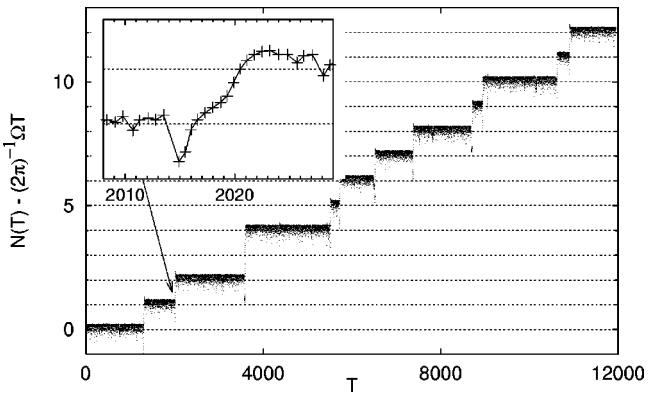

FIG. 15. Temporal development of difference between phases of the driven system and the driving force in the state of imperfect phase synchronization. $E=10$, $\Omega=8.3$; crosses denote intersections with Poincaré surface.

phase range) and the sharp and relatively dense ''whiskers'' as well as the surrounding cloud in the border regions. Apparently, in the course of evolution the system spends most of the time in the central region; from time to time it drifts along the whiskers to the identical pattern which is shifted along the phase by 2π. Further, we will attempt to interpret this dynamics with the help of the information about the embedded periodic orbits.

Similarly to the case $r=210$, we have located on the parameter plane the main Arnold tongues for individual periodic orbits (Fig. 14). In the autonomous system the number of periodic orbits of the length l rapidly grows with the increase of l: there are such 224 orbits with $l\leqslant 10$; even taking into account the mirror symmetry of the system due to which all periodic orbits with odd length and most of those with even length have symmetric twins, these orbits still deliver 116 different main Arnold tongues. Presenting all of them within a single plot hardly makes sense. We show only the principal phase locking regions which correspond to typical periodic orbits at the left and the right ends of the frequency band; as long as the forcing amplitude remains moderate, the rest of the main Arnold tongues appears to be lying between the plotted ones.

According to the results presented in Fig. 14, there is a large domain on the parameter plane in which all (or nearly all) main Arnold tongues overlap. Following the discussion in the preceding sections, one would expect to observe in this domain the state of perfect phase synchronization. However, this is not the case, and even the states which we denote as imperfectly synchronized occupy only a part of the overlapping region. It appears that to determine only the main Arnold tongues is insufficient for the explanation of the entire picture; some additional information is apparently required.

Let us follow the temporal development of difference between the phase of the system and the phase of the external force. As can be seen from Fig. 15, this difference plotted against time resembles a staircase in which the relatively long horizontal ''stairs'' alternate with short jumps. (We plot, in fact, the phase difference divided by 2π or, in other words, the difference between the number of intersections with the Poincaré plane and the number of periods of external force.) The entire plotted interval contains 16 000 orbit turns.

Each stair corresponds to a segment of synchronized motion (minor oscillations around the horizontal line are caused by our arbitrariness in the choice of the Poincaré surface; they compensate each other in the net effect), and the jumps between the stairs look like occasional phase slips. At the starting point the system and the driving force are assigned the same phase value; within the first stair they remain in phase; within the second stair the driving force has a phase lag of 2π or, in other words, of one period; within the third stair the time lag equals two periods of external force, and so on. In the course of long-time evolution, we observe not only 2π but also 4π jumps; the latter are, however, much more seldom. Noticeably, each jump upwards is preceded by a short local decline downwards; this indicates that immediately before the jump the phase trajectory rotates relatively slow.

Let us now zoom in on the vicinity of a typical jump (inset of Fig. 15). Here, the crosses denote the moments of intersections with the Poincaré surface; between them, the phase of the trajectory is approximated by linear interpolation. We observe that what seemed to be an instantaneous phase slip proves to be a kind of phase drift, a process of noticeable duration: a transition between two stairs requires not fewer than a dozen turns of the orbit. In the temporal pattern of the transition one sees a remarkably long-time interval between two intersections of the Poincaré plane in the very beginning of the transition process; this interval is produced by a very slow orbit turn. This slowing down is followed by several very short intervals; they not only enable the system to compensate the local phase lag accumulated during the slow motion, but even catapult it upwards to the next stair. The whole picture reminds us of the unstable periodic orbits which belong to the upper branch of the frequency distribution displayed in Fig. 9, with their slow passages near the saddle origin and subsequent rapid rotations around the saddle foci. The high individual frequencies of these orbits by far exceed the average frequency $\omega_a=8.365$; consequently, not only their main locking regions are relevant, but also certain secondary Arnold tongues can be of importance.

Take a periodic orbit which consists of l turns and has in the autonomous case the individual frequency ω_i. For l sufficiently high, the value $[(l-1)/l]\omega_i$ (which corresponds to the situation when the orbit closes not after l but after $l-1$ periods of the external force) also lies inside the band of individual frequencies, and the corresponding Arnold tongue

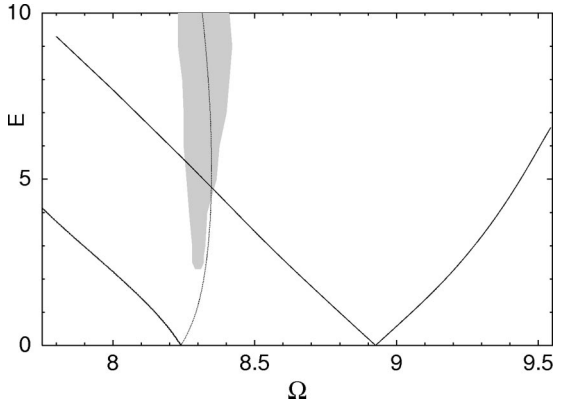

FIG. 16. Main locking region (right) and the region of locking 12:13 (left) for the periodic orbit of length 13. Gray domain: region of imperfect phase synchronization.

can be of relevance. Formally, this may hold for any frequency distribution, but in the case of a narrow frequency band the value of l should be rather high (for the nearly monochromatic attractor from Sec. III one would require $l>500$), and the chance to stay long enough near the very long unstable periodic orbit is negligible. On the contrary, in the case of $r=28$ this phenomenon can be detected already for $l=12$ (the estimate is based on the values of ω_i of the autonomous system; since the Arnold tongues in the forced system have finite width, the actual values of l may be slightly lower). For most of the time the trajectory on the attractor wanders between unstable tori whose phase-stable orbits are directly locked to the frequency of the driving force, but now and then it visits neighborhoods of tori whose frequencies are locked in a ratio $(l-1)/l$. During these visits, the phase of the orbit grows faster than that of the external force; by the time when the trajectory is bounced back, a total gain of 2π is reached. Similarly, the phase gains of 4π can be interpreted as rare passages of a chaotic trajectory near the periodic orbits locked in the frequency ratio $(l-2)/l$; in our case, these orbits should have a length $l\geqslant 21$.

The described phenomenon is a ''masked'' form of phase synchronization: the observed gains (or losses) of the phase do not result from instantaneous phase slips. Although the difference $\omega-\Omega$ does not vanish in this state, the motion remains synchronized for all the time, but synchronized to *different* frequencies.

As an example we take an orbit of length 13 which makes one slow turn in the half-space $x>0$ and 12 fast turns in the half-space $x<0$ (cf. Fig. 10); its individual frequency in the autonomous system equals $\omega_i=8.925\,918\ldots$. Besides the main Arnold tongue emanating from ω_i, the other locking region is of apparent interest for us: it corresponds to the situation in which the periodic orbit is closed after 12 periods of external force. This secondary Arnold tongue has its tip in the point $(\omega=12/13\,\omega_i=8.239\,367\ldots, E=0)$, and lies much closer to ω_a. Therefore we can expect that in the range of frequency values corresponding to plateaus of Fig. 12 the considered unstable periodic orbit is locked by external force in a ratio 12:13. A passage of a chaotic trajectory near this synchronized orbit would cause a net phase gain of 2π and result in a transition to a higher stair in a plot of Fig. 15.

In Fig. 16 we present two described Arnold tongues for the periodic orbit of length 13. As can be seen, the tongues overlap at $E\geqslant 4.68$; the adjacent area in the parameter plane belongs to the region in which imperfect phase synchronization is observed. In this parameter domain we detect the coexistence of two different phase-stable periodic orbits, both of which stem from the same unstable periodic solution of the autonomous system. One can expect that in the course of sufficiently long evolution a chaotic trajectory will visit the neighborhoods of both orbits; in one of these neighborhoods it will keep pace with the phase of external force, whereas in the other it will eventually run 2π ahead of it. Notably, two periodic orbits with different winding numbers cannot be simultaneously placed onto a surface of a single two-torus (produced by action of the forcing from the ''parental'' periodic solution of the autonomous system); this implies that already the moderate amplitudes of forcing can cause a breakup of invariant tori.

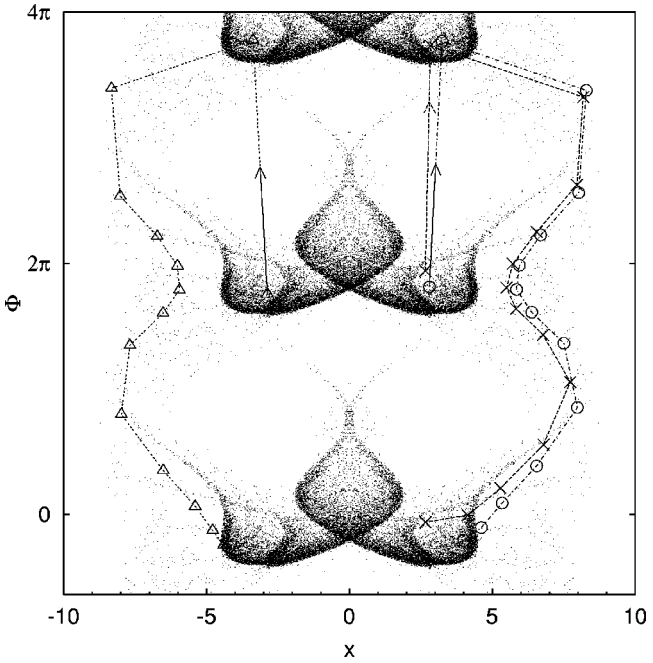

FIG. 17. Periodic orbits and the attractor in the state of imperfect synchronization. Dots, chaotic trajectory; crosses, periodic orbits locked in the ratio 12:13; circles, periodic orbits locked in the ratio 13:14; triangles, periodic orbits locked in the ratio 14:15. Arrows show the direction of motion along the orbit. $E=10$, $\Omega=8.3$.

To provide a geometric illustration of the described phenomenon, we plot in Fig. 17 the attractor of the Poincaré map on the secant plane. The marked points denote the unstable periodic orbits of the length l for $l=13$, $l=14$, and $l=15$ which are frequency locked in the ratio $(l-1)/l$. It can be seen that these points can be found both in the bulk of the attractor and in the ''whiskers.'' The chaotic orbit which approaches one of such orbits inside the bulk makes with it an excursion downwards along the whisker and is transported into the bulk of identical pattern which is shifted along ϕ by 2π.

Now we can interpret the origin of short nonflat plateaus in Fig. 12 as the complicated interplay between the main Arnold tongues of relatively short periodic orbits and the secondary locking regions of occasionally visited longer orbits. When the driving frequency Ω is increased from the low starting value, the motions on the tori born out of short

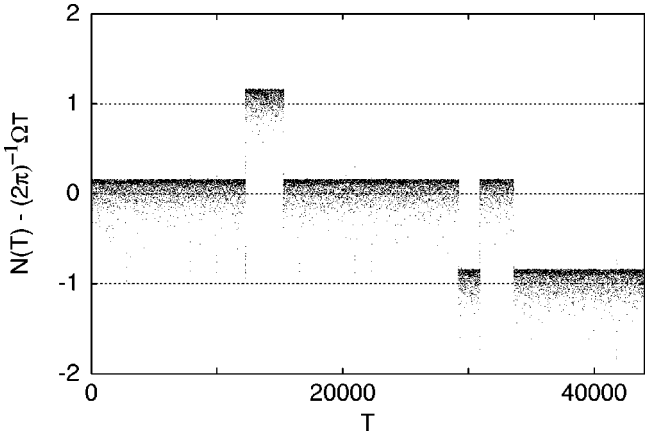

FIG. 18. Temporal evolution of difference between phases of the driven system and the driving force: $r=28$, $E=14$, and $\Omega=8.25$. The plotted segment corresponds to 6×10^4 turns of the orbit.

orbits are not yet locked in their main Arnold tongues, and the frequency of rotations near these tori is larger than Ω. In this parameter range the secondary lockings for longer orbits can be encountered; since their locking ratios are smaller than 1, the frequencies of locked motions upon them also exceed Ω. Altogether, this ensures that the inequality $\omega-\Omega>0$ holds. Further, we enter the parameter region in which most of the short orbits have their main Arnold tongues. As soon as we reach the values of Ω at which the motions near the locked short orbits dominate, the state of imperfect phase synchronization is observed. Formally, we can write $\omega=\kappa\Omega$ where the factor κ is a (not everywhere differentiable) function of Ω; κ remains constant inside the small intervals of Ω in which no crossings of the tongue borders occur. Due to the contribution of secondary lockings, in this parameter range one has $\kappa(\Omega)>1$; hence inside such intervals the function $\omega-\Omega=\Omega(\kappa-1)$ is increasing; this explains the nonmonotonicity of synchronization plateaus.

Finally, in the course of an increase of Ω, we cross one by one the right boundaries of both the main and the secondary Arnold tongues. In the vicinities of the respective just-out-of-locking tori, the phase of a chaotic trajectory grows slower than the phase of the driving force. As a consequence, the rare segments of drift downwards start to appear in the time dependence of the difference between these phases. These shifts downwards eventually balance (cf. Fig. 18), and finally exceed the effect of rare shifts upwards caused by still surviving secondary tongues; this marks the end of the region of imperfect synchronization.

V. DISCUSSION

The ''imperfections'' in phase synchronization which we have discussed in the previous section do not signify the breakdown of synchronized state. Although the formal condition $\Omega=\omega$ does not hold, the system appears to be phase locked all the time, but the values of locking ratios alternate in the course of chaotic evolution. A similar phenomenon of nonconstant locking ratios in phase synchronization has been recently detected in the experimental data describing human cardiorespiratory activity [46,47]. There the switchings between the ratios are apparently owing to the influence of noise and to the nonstationarity of the process. Our results imply that alternation of locking ratios can also take place in a completely stationary deterministic setup, under the provision of the broad distribution of return times.

In the first lines of this paper, we have interpreted synchronization as the adjustment of coupled subsystems. Adjustment is tantamount to introducing some kind of order into the dynamics: all known forms of chaotic synchronization are known to decrease the degree of chaoticity. Geometrically, synchronization manifests itself in the reduction of dynamics from the entire phase space onto some attracting invariant hypersurface; in the case of complete synchronization this is an explicitly given symmetrical hyperplane whereas in the case of generalized synchronization the surface is determined by the functional interrelation between the leading and the led subsystems. The case of phase synchronization is less transparent, owing to the hardly avoidable ambiguities in the definition of the phase. Nevertheless, as can be seen from the comparison of Fig. 6(a) and Fig. 6(c), there is no doubt that the portion of phase space occupied by the attractor in the perfectly synchronized state is much smaller than in the absence of synchronization. The measured phase of the system, being adjusted to the phase of the driving force, does not follow it minutely, and the attractor in Fig. 6(c) remains a stripe of a finite width which does not shrink into a curve. The loose relation between the phases defines the geometry of the attracting ''fat'' hypersurface. For the case of imperfect phase synchronization, however, the picture seems to be more complicated. In the temporal evolution the prevailing long segments of frequency locking 1:1 are interrupted by short time intervals in which the frequencies, albeit rationally locked, do not coincide. Each locking defines its own invariant ''hypersurface''; accordingly, in the phase space the trajectory moves for a long time along one (''main'') surface, for a short time leaves it and makes an excursion along the other surface, and so on. The already mentioned fact that phase is usually a ''hidden'' variable makes especially difficult a proper characterization of this unconventional ordered state, either through reconstruction of the underlying invariant geometric structures, or by other means; the corresponding methods require further elaboration.

Another problem which deserves attention in this context is the breakup of unstable tori under the increase of the forcing amplitude, and the consequences of this breakup for the phase synchronization. Further, unstable periodic orbits in autonomous systems can have structurally stable homoclinic and heteroclinic orbits; the effects of periodic perturbation of respective homoclinic structures (for example, existence of additional connections between phase-unstable and phase-stable orbits in the locking regions) demand a special investigation. These fine aspects remain outside our current descriptive approach; however, their elucidation by means of a more rigorous analysis can add new important details to our understanding of the synchronization phenomena.

ACKNOWLEDGMENTS

We are grateful to A. Pikovsky, M. Rosenblum, and G. Osipov for stimulating discussions. The research of E.-H.P. was partially supported by the Korea Science and Engineering Foundation. M.Z. acknowledges the support of the Max-Planck Gesellschaft and SFB-555.

[1] C. Hugenii, *Horoloqium Oscilatorium* (Iowa State University Press, Ames, 1986).
[2] C. Hayashi, *Nonlinear Oscillations in Physical Systems* (McGraw-Hill, New York, 1964).
[3] I. I. Blekhman, *Synchronization in Dynamical Systems* (Nauka, Moscow, 1971).
[4] H. Fujisaka and T. Yamada, Prog. Theor. Phys. **69**, 32 (1983).
[5] A. S. Pikovsky, Z. Phys. B: Condens. Matter **55**, 149 (1984).
[6] L. M. Pecora and T. L. Carroll, Phys. Rev. Lett. **64**, 821 (1990).
[7] C. Tresser, P .A. Worfolk, and H. Bass, Chaos **5**, 693 (1995).
[8] N. F. Rulkov, M. M. Sushchik, L. S. Tsimring, and H. D. I. Abarbanel, Phys. Rev. E **51**, 980 (1995).
[9] H. D. I. Abarbanel, N. F. Rulkov, and M. M. Sushchik, Phys. Rev. E **53**, 4528 (1996).
[10] L. Kocarev, and U. Parlitz, Phys. Rev. Lett. **76**, 1816 (1996).
[11] M. G. Rosenblum, A. S. Pikovsky, and J. Kurths, Phys. Rev. Lett. **76**, 1804 (1996).
[12] D. Gabor, J. IEE London **93**, 429 (1946).
[13] A. S. Pikovsky, M. G. Rosenblum, G. V. Osipov, and J. Kurths, Physica D **104**, 219 (1997).
[14] A. S. Pikovsky, M. A. Zaks, M. G. Rosenblum, G. V. Osipov, and J. Kurths, Chaos **7**, 680 (1997).
[15] E. R. Rosa, E. Ott, and M. H. Hess, Phys. Rev. Lett. **80**, 1642 (1998).
[16] P. W. Milonni, J. R. Ackerhalt, and H. W. Galbraith, Phys. Rev. A **28**, 887 (1983).
[17] A. G. Vladimirov and D. Yu. Volkov, Opt. Commun. **100**, 351 (1993).
[18] R. Herrero, J. Farjas, R. Pons, F. Pi, and G. Orriols, Phys. Rev. E **57**, 5366 (1998).
[19] J. A. Yorke, E. D. Yorke, and J. Mallet-Paret, Physica D **24**, 279 (1987).
[20] M. R. E. Proctor and N. O. Weiss, Nonlinearity **3**, 619 (1990).
[21] A. M. Rucklidge, J. Fluid Mech. **237**, 209 (1992).
[22] B. A. Malomed and A. A. Nepomnyashchy, Phys. Rev. A **42**, 6238 (1990).
[23] M. A. Zaks, A. A. Nepomnyashchy and B. A. Malomed, Phys. Scr. **T67**, 143 (1996).
[24] E. N. Lorenz, J. Atmos. Sci. **20**, 130 (1963).
[25] E. Ott, *Chaos in Dynamical Systems* (Cambridge University Press, Cambridge, England, 1993).
[26] D. Auerbach, P. Cvitanović, J.-P. Eckmann, G. Gunaratne, and I. Procaccia, Phys. Rev. Lett. **58**, 2387 (1987).
[27] R. Artuso, E. Aurell, and P. Cvitanović, Nonlinearity **3**, 325 (1990).
[28] R. Artuso, E. Aurell, and P. Cvitanović, Nonlinearity **3**, 361 (1990).
[29] P. Cvitanović, Physica D **51**, 138 (1991).
[30] C. Grebogi, E. Ott, and J. A. Yorke, Phys. Rev. A **36**, 3522 (1987).
[31] D. P. Lathrop and E. J. Kostelich, Phys. Rev. A **40**, 4028 (1989).
[32] D. Pierson and F. Moss, Phys. Rev. Lett. **75**, 2124 (1995).
[33] X. Pei and F. Moss, Nature (London) **379**, 618 (1996).
[34] P. So, E. Ott, T. Sauer, B. J. Gluckman, C. Grebogi, and S. J. Schiff, Phys. Rev. E **55**, 5398 (1997).
[35] P. So, E. Ott, S. J. Schiff, D. T. Kaplan, T. Sauer, and C. Grebogi, Phys. Rev. Lett. **76**, 4705 (1996).
[36] S. M. Zoldi and H. S. Greenside, Phys. Rev. E **57**, R2511 (1998).
[37] E. Ott, C. Grebogi, and J. A. Yorke, Phys. Rev. Lett. **64**, 1196 (1990).
[38] V. Francheschini, C. Giberti, and Z. Zheng, Nonlinearity **6**, 251 (1993).
[39] B. Eckhardt and G. Ott, Z. Phys. B: Condens. Matter **93**, 259 (1994).
[40] B. R. Hunt and E. Ott, Phys. Rev. Lett. **76**, 2254 (1996).
[41] S. M. Zoldi and H. S. Greenside, Phys. Rev. Lett. **80**, 1790 (1998).
[42] B. R. Hunt and E. Ott, Phys. Rev. Lett. **80**, 1791 (1998).
[43] A. S. Pikovsky, G. V. Osipov, M. G. Rosenblum, M. A. Zaks, and J. Kurths, Phys. Rev. Lett. **79**, 47 (1997).
[44] C. Sparrow, *The Lorenz Equations: Bifurcations, Chaos, and Strange Attractors* (Springer, New York, 1982).
[45] Close to the homoclinic bifurcation the dynamics is reducible to the one-dimensional mapping $\xi_{i+1}=\xi_i^{-\lambda_s/\lambda_u}-\mu$ where μ is proportional to the distance from the bifurcational parameter value (see, e.g., [44]). For $\mu\to 0$ under positive ν the eigenvalue of the fixed point of this mapping tends to $\approx -\lambda_s/\lambda_u \times \mu^{1+\lambda_u/\lambda_s}$.
[46] C. Schäfer, M. G. Rosenblum, J. Kurths, and H.-H. Abel, Nature (London) **392**, 239 (1998).
[47] C. Schäfer, M. G. Rosenblum, H.-H. Abel, and J. Kurths, Phys. Rev. E **60**, 857 (1999).